

Runx2 stabilizes hypoxia-inducible factor-1 α through competition with pVHL and stimulates angiogenesis in growth plate hypertrophic chondrocytes

Sun Hee Lee¹, Xiangguo Che³, Jae-Hwan Jeong³, Je-Yong Choi³, Young-Joo Lee⁴, Yong-Hee Lee⁵,
Suk-Chul Bae⁵, and You Mie Lee^{1,2}

¹School of Life Sciences and Biotechnology, College of Natural Sciences, ²Research Institute of Pharmaceutical Sciences, College of Pharmacy, ³School of Medicine, Kyungpook National University, Daegu, ⁴Department of Bioscience and Biotechnology, Sejong University, Seoul, ⁵School of Medicine, Chungbuk National University, Cheongju, South Korea

*Running title: *Runx2 stabilizes HIF-1 α*

To whom correspondence should be addressed: You Mie Lee, Ph.D., College of Pharmacy, Kyungpook National University, Daegu, 702-701, Republic of Korea. Tel: +82-53-950-8566, Fax: +82-53-950-8557, E-mail: lym@knu.ac.kr.

Keywords: Runx2; HIF-1 α ; hypertrophic chondrocyte; endochondral bone formation

Background: Runx2-related transcription factor 2 (Runx2) is a key factor in bone development. Hypoxia-inducible factor-1 α (HIF-1 α) is the primary regulator of blood vessel formation.

Results: Runx2 bound and activated HIF-1 α by competing with Von Hippel-Lindau protein (pVHL), protecting HIF-1 α from degradation.

Conclusion: Runx2 stabilizes HIF-1 α during endochondral bone formation.

Significance: Runx2/HIF-1 α stimulate the invasion of blood vessels in hypertrophic zones.

SUMMARY

The regulation of hypoxia-inducible factor-1 α (HIF-1 α) during endochondral bone formation is not fully understood. Here, we investigated the cross-talk between HIF-1 α and runt-related transcription factor 2 (Runx2) in the growth plate. Runx2 caused the accumulation of HIF-1 α protein in ATDC5 chondrocytes and HEK293 cells under normoxic conditions. Runx2 also increased the nuclear translocation of HIF-1 α when coexpressed in HEK293 cells and interacted with HIF-1 α at the oxygen-dependent degradation domain (ODDD). In addition, Runx2 competed with Von Hippel-Lindau tumor suppressor protein (pVHL) by directly binding to ODDD-HIF-1 α and significantly

inhibited the ubiquitination of HIF-1 α , even though Runx2 did not change the hydroxylation status of HIF-1 α . Furthermore, overexpression of Runx2 resulted in the significant enhancement of vascular endothelial growth factor (VEGF) promoter reporter activity and protein secretion. Runx2 significantly increased angiogenic activity in human umbilical vein endothelial cells *in vitro*. In wild-type mice, HIF-1 α and Runx2 were colocalized in hypertrophic chondrocytes in which the cluster of differentiation 31 (CD31) protein was expressed at embryonic day 15.5 (E15.5). In contrast, the expression of HIF-1 α was markedly reduced in areas of CD31 expression in Runx2^{-/-} mice. These results suggest that Runx2 stabilizes HIF-1 α by binding to ODDD to block the interaction between pVHL and HIF-1 α . In conclusion, Runx2, HIF-1 α and VEGF may regulate vascular angiogenesis spatially and temporally in the hypertrophic zone of the growth plate during endochondral bone formation.

The development of new capillaries in developing organs is essential for the supply of oxygen and nutrients (1, 2). An interesting feature of developing embryos is the high level of vascularization achieved through the upregulation of vascular endothelial growth factor (VEGF) as

a result of the transactivation of hypoxia-inducible factor-1 (HIF-1) (2). Endochondral bone formation takes place in the growth plate, a highly specialized organ that generates the majority of longitudinal growth until adulthood (3, 4). Bone formation here begins with the aggregation of mesenchymal cells and their differentiation into chondrocytes. Chondrocyte hypertrophy, which initiates in the center of cartilaginous skeletal elements, drives longitudinal bone growth. Hypertrophy is characterized by an increase in cellular volume and the expression of specific extracellular matrix components, including collagen type X, a commonly used marker for this state (4, 5). Chondrocyte hypertrophy is followed by apoptosis, invasion of blood vessels, osteoclasts and other mesenchymal cells from the perichondrium, and the production of the mature bone matrix. The ultimate size and structure of each endochondral bone depends on the coordinated regulation of chondrocyte proliferation, maturation and hypertrophy in response to multiple extracellular signals (6, 7). Interestingly, the blood vessel disruption of the growth plate reduces bone mineralization and the replacement of hypertrophic chondrocytes (8, 9), suggesting that bone formation is largely dependent on vascularization.

VEGF expressed in hypertrophic chondrocytes is required for chondrocyte survival and cartilage angiogenesis (10, 11, 12). Cartilage is an avascular organ, with the exception of hypertrophic chondrocytes, which become a target for capillary invasion and angiogenesis during developmental endochondral ossification (4, 13). Hypertrophic chondrocytes may produce angiogenic activators, whereas other types of cartilage produce angiogenic inhibitors (14). A delicate balance between the formation and vascularization rates of calcified cartilage must be maintained in order for bone development to proceed normally.

The HIF-1 transcriptional complex plays an essential role in cellular and systemic oxygen homeostasis (15, 16). Under hypoxic conditions, the various target genes involved in angiogenesis, cell survival, the glycolytic pathway and apoptosis are upregulated by HIF-1 (16). An α -

subunit of HIF-1 (HIF-1 α) heterodimerizes with its constitutively expressed binding partner, aryl hydrocarbon receptor nuclear translocator (ARNT, or HIF-1 β), a common binding partner of several basic helix-loop-helix (bHLH)-Per-ARNT-Sim (PAS) domain proteins (17). Under normoxic conditions, HIF-1 α is rapidly degraded by the ubiquitin-proteasome pathway (18). Ubiquitination of HIF-1 α is mediated by interaction with the Von Hippel-Lindau protein (pVHL), a tumor suppressor (19). The association of HIF-1 α with pVHL is in turn triggered by the post-translational hydroxylation of proline residues, mediated by prolyl hydroxylase (PHD) or HIF prolylhydroxylase (HPH). Proline hydroxylation of Pro 402 and Pro 564 in the oxygen-dependent degradation domain (ODDD) (20) recruits the pVHL E3 ubiquitin-protein ligase complex to HIF-1 α and targets HIF-1 α for degradation (21).

HIF-1 α is expressed in the entire region of developing chondrocytes, and ablation of HIF-1 α results in embryonic lethality, with massive chondrocyte apoptosis (11, 22). Hypoxia is a major stimulator of angiogenesis during endochondral bone formation. The mesenchymal cells of presumptive endochondral bones and the fetal growth plate are hypoxic and express HIF-1 α (22-24). It has also been found that HIF-1 α is required for the survival of hypoxic chondrocytes. Furthermore, it has been proposed that HIF-1 α is a major regulator of the gene programs that orchestrate angiogenesis and osteogenesis coupling (25).

Mammalian runt-related genes include *RUNX1*, *RUNX2* and *RUNX3*. Runt-related transcription factor 2 (Runx2) activity promotes the expression of a number of osteogenic markers by binding to responsive elements within the promoters of type I collagen, osteopontin and osteocalcin (26). The zinc finger transcription factor osterix acts downstream of Runx2 and is required for osteoblast differentiation and bone formation (27). Furthermore, heterozygous mutations in Runx2 cause the human autosomal dominant bone disease, cleidocranial dysplasia (CCD) (28). Runx2-deficient mice have been shown to undergo defective hypertrophic chondrocyte differentiation in some skeletal

elements, suggesting that Runx2 may regulate chondrocyte hypertrophy (29). In addition, it has been reported that Runx2 increases VEGF transcription in hypertrophic chondrocytes during bone development (30). However, whether Runx2 regulates HIF-1 α in hypertrophic chondrocytes during bone formation in normoxic regions is largely unknown.

Here, we show for the first time that Runx2 enhances the stability and transcriptional activity of HIF-1 α by interacting with the ODDD and competing with pVHL to inhibit ubiquitination. Ectopic expression of Runx2 also increases both the transcription and secretion of VEGF. Moreover, Runx2 overexpression enhanced *in vitro* and *in vivo* angiogenesis through enhanced secretion of VEGF. In addition, hypertrophic chondrocytes associated with the developing bone of Runx2 knockout mice demonstrated decreased expression of both HIF-1 α and cluster of differentiation 31 (CD31) protein. Taken together, these results support a mechanism by which Runx2-mediated HIF-1 α accumulation in hypertrophic chondrocytes stimulates the expression of VEGF, even in the normoxic region, and encourages the invasion of microvessels during endochondral bone formation.

EXPERIMENTAL PROCEDURES

Reagents and Antibodies - Cyclohexamide (CHX) and MG132 were purchased from Sigma (St. Louis, MO, USA). Mouse monoclonal antibodies against HIF-1 α and α -tubulin were purchased from BD Biosciences (San Diego, CA) and Zymed (South San Francisco, CA), respectively. Mouse monoclonal antibodies against c-Myc (Myc), hemagglutinin (HA) and green fluorescent protein (GFP) were purchased from Santa Cruz Biotechnology (Santa Cruz, CA). Runx2 antibody was purchased from Novus Biologicals (Littleton, CO).

Animals and genotyping - Animal care and experiments were performed in accordance with the Institutional Guidelines of the Animal Care and Use Committees of Kyungpook National University. Animals were maintained on a 12 h-light–12 h darkness cycle at 22 °C to 25 °C under specific-pathogen-free (SPF) conditions and fed

with standard chow and water *ad libitum*. Genotyping of Runx2 null and heterozygote mice was performed as previously described (31).

Plasmids - The pcDNA3-HA-pVHL plasmid contains the pVHL coding sequence inserted into pcDNA3. The pCS4-3HA-Runx2 and pCS4-3Myc-Runx2 plasmids were generated by Dr. Suk-Chul Bae (Chungbuk National University, Korea). The pEBG-HIF-1 α (glutathione-S-transferase (GST)-HIF-1 α) and truncated pEBG-HIF-1 α plasmids were obtained from Dr. Kyu Won Kim (Seoul National University, Seoul, Korea).

Cell culture and hypoxic conditions - Human embryonic kidney cells (HEK293 cell line) were maintained in Dulbecco's Modified Eagle's Medium (DMEM) (Hyclone, Logan, UT) supplemented with 10% fetal bovine serum (FBS) (Hyclone) and 1% antibiotics (100 units/ml penicillin, 100 μ g/ml streptomycin, Invitrogen). Human umbilical vein endothelial cells (HUVECs, passage 2 to 5) were grown on 1% gelatin-coated culture plates in M199 medium (Hyclone) supplemented with 20% FBS and 1% antibiotics (complete medium). Runx2-overexpressing ATDC5 chondrocytes were provided by Dr. Dae-Won Kim (Yonsei University, Seoul, Korea). ATDC5 cells were cultured in DMEM/F12 (1:1) hybrid medium (Hyclone) supplemented with 5% FBS, 10 μ g/ml human transferrin (Sigma) and 3 x 10⁻⁸ M sodium selenite (Sigma). For the hypoxic condition, the cells were incubated in 5% CO₂ with 1% O₂ balanced with N₂ in a hypoxic chamber (Astec, Fukuoka, Japan) at 37 °C.

Transient transfection - For the overexpression of Runx2, HIF-1 α and pVHL expression plasmids, subconfluent HEK 293 cells were transiently transfected with mock, Runx2, HIF-1 α or pVHL plasmids using the WelFect-EXTM transfection reagent (WelGene, Daegu, Korea) according to the manufacturer's protocol.

Luciferase assay - For luciferase assays, HEK 293 cells were transfected with appropriate combinations of effector plasmids (reporter plasmid HRE-Luc, control plasmid pCMV- β -gal and experimental plasmid pCS4-3HA-Runx2) using the WelFect-EXTM transfection reagent (WelGene) according to the manufacturer's

protocol. After transfection, the cells were harvested, and extracts were prepared using reporter lysis buffer (Promega, Madison, WI). Cell lysates were analyzed for luciferase activity using the luciferase assay kit (Promega) and a luminometer (Turner Designs, Sunnyvale, CA). The cell extracts were assayed using the β -galactosidase enzyme assay kit (Promega). Each extract was assayed three times. The relative luciferase activity was calculated as relative luciferase units (RLU)/ β -galactosidase activity.

Reverse transcription-polymerase chain reaction

(RT-PCR) - Total RNA was isolated from the cells by a single-step procedure with TRIzol Reagent (Invitrogen, Carlsbad, CA). cDNA was synthesized with MMLV-reverse transcriptase (RT) (Promega) and oligo-dT primers. PCR reactions were performed with the first strand cDNAs using a PCR reaction kit (Takara, Ostu, Japan) and the primer sets described below. Amplification by PCR was performed using an automated thermal cycler (BioRad, Hercules, CA). Oligonucleotide primers for PCR were designed as follows: β -actin, 5'-GACTACCTCATGAAGATC-3' and 5'-GATCCACATCTGCTGGAA-3'; HIF-1 α , 5'-CAGAAGATAACAAGTAGCCTC-3' and 5'-CTGCTGGAATACTGTAAGT-3'; VEGF, 5'-GAGAATTCGGCCTCCGAAACCATGAACTTCTGT-3' and 5'-GAGCATGCCCTCCTGCCCGGCTCACCGC-3'; arrest-defective-1 protein (ARD1), 5'-AGTTGTTTCGATATGGTGAG-3' and 5'-TCTGCTACAGGGAAAACAGT-3'; prolyl hydroxylase domain-containing protein (PHD) 1, 5'-ATGGACAGCCCGTGCCAGCCGCA-3' and 5'-CGCAGCTCACCACCATCCTGCCC-3'; PHD2, 5'-ATGGCCAGTGACAGCGGC-3' and

5'-CAACGGCTTGGTCTGCCC-3'; PHD3, 5'-ATGCCTCTGGGACACATC-3' and 5'-TCAGTCTTTAGCAAGAGCA-3'; glucose transporter 1 (Glut1), 5'-TACCCTGGATGTCCTATCTG-3' and 5'-CACACAGTTGCTCCACATAC-3'; enolase, 5'-GGTGGATCTCTATACTGCCA-3' and 5'-CTTTGCCCTAAGTAACGCTGT-3'; and aldolase C, 5'-TGAGCAGAAGAAGGAGTTGT-3' and 5'-GGTCTCATGGAAGAAAATGA-3'.

Co-immunoprecipitation and Western blot analysis

- At 24 h post-transfection, the cells were exposed to normoxic or hypoxic conditions. The cell pellets were lysed with cell lysis buffer (20 mM Tris (pH 7.5), 150 mM NaCl, 1 mM EDTA, 1% Triton X-100, and 1X protease inhibitor cocktail) supplemented with 1 mM PMSF and incubated for 10 min. The mixtures were centrifuged at 15,000 rpm for 20 min. Total cell lysates were incubated with the appropriate antibody overnight. A 50% slurry of protein A/G agarose beads (Pierce, Woburn, MA) was added to each reaction mixture and incubated for 3 h with gentle rocking. Co-immunoprecipitated proteins were separated by sodium dodecyl sulfate polyacrylamide gel electrophoresis (SDS-PAGE) and transferred to a nitrocellulose membrane (Whatman, Maidstone, England). The membrane was blocked with 5% non-fat skim milk in Tris-buffered saline containing 0.1% Tween-20 (TBST). Subsequently, the membrane was incubated with the appropriate primary antibody overnight, followed by incubation with horseradish peroxidase-conjugated mouse or rabbit antibodies for 1 h; the blots were then developed with the West Pico Chemiluminescent Substrate (Pierce).

Conditioned media (CM) preparation - To perform angiogenesis assays *in vitro*, CM was collected from transfected cells expressing either Runx2 plasmid or the control plasmid. Subconfluent cells were transiently transfected with HA- or Myc-tagged Runx2 plasmids in the pCS4 vector (pCS4-3HA-Runx2, pCS4-3Myc-Runx2) for 4 h and then stabilized in fresh

complete medium for 24 h. The medium was replaced with M199 containing 1% FBS without growth factors to collect CM.

Fractionation of cytosolic and nuclear proteins - The cells were washed with ice-cold phosphate buffered saline (PBS) and harvested in 500 μ l lysis buffer A (10 mM HEPES (pH 7.9), 10 mM KCl, 0.1 mM EDTA, 1 mM DTT, 0.5 mM PMSF, 1% NP-40). After incubation for 15 min at 4 °C, the cytosolic protein fraction was separated by centrifugation at 13,000 rpm for 5 min. After the cytosolic fraction was obtained, lysis buffer B (20 mM HEPES (pH 7.9), 0.4 M NaCl, 1 mM EDTA, 1 mM DTT, and 1 mM PMSF) was added to the cell pellet, and the mixture was vortexed for 30 min. Nuclear fractions were separated by centrifugation at 15,000 rpm for 10 min, and the two fractions were subjected to SDS-PAGE and western blot analysis.

In vitro protein binding assay - For the *in vitro* protein binding assay, pEGFP-HIF-1 α , pCS4-3HA-Runx2, or pcDNA3-HA-pVHL were individually overexpressed in HEK293 cells. The pEGFP-HIF-1 α cell lysate was incubated with pCS4-3HA-Runx2 cell lysate for 3 h and then incubated with pcDNA3-HA-pVHL cell lysate at 4 °C for 3 h. After immunoprecipitating with anti-GFP-conjugated magnetic beads, HIF-1 α binding proteins were analyzed by the immunoblot assay using an anti-HA antibody.

Immunofluorescence assay - The cells that were seeded onto coverslips were fixed with 10% paraformaldehyde solution and prepared for the immunofluorescence assay, as previously described (32). Briefly, following incubation with primary antibody, the cells were incubated with FITC-conjugated and Texas Red-conjugated secondary antibodies and mounted onto microscope slides with a DAPI mounting solution. Fluorescent images of the cells were obtained and analyzed with a Zeiss fluorescence microscope (Zeiss, Oberkochen, Germany).

Cell proliferation assay - Proliferation of HUVECs was assayed as previously described (33). CM was used after starvation with low serum medium (1% FBS in M199). The cell-associated radioactivity was then determined using a liquid scintillation counter (PerkinElmer,

USA).

Cell migration assay - Migration was measured using 24-well transwell units with polycarbonate filters with a 8 μ m pore size (Costar, Lowell, MA), as previously described (33). The lower compartment contained 600 μ l CM, and 5 x 10⁴ cells were resuspended in 100 μ l DMEM and placed in the upper part of a transwell plate. The cells were incubated in a humidified atmosphere of 5% CO₂ at 37 °C for 16 h. The cells were fixed with methanol and stained with hematoxylin (Sigma) and eosin (Sigma). Cells on the upper surface of the filter were removed and counted under a light microscope at 400X magnification. Each sample was assayed in triplicate, and each assay was repeated twice.

Tube formation assay - HUVECs were seeded onto 24-well culture plates pre-coated with Matrigel (10 mg/ml, BD Biosciences) for 30 min at 37 °C. CM from HEK293 cells transiently transfected with mock control and Runx2 plasmids was added, and the cells were incubated for 24 h. Morphologic changes of the cells were observed under a microscope and photographed at 40X magnification.

Immunohistochemistry - Hypoxic probe-1 (pimonidazol HCl, Chemicon International, Temecula, CA) was injected 4 h before tissue dissection. The lower limbs of embryonic day 15.5 (E15.5) embryos were fixed with 4% paraformaldehyde in PBS and dehydrated, embedded in paraffin, cut into 5 μ m sections and processed for either histology or immunohistochemistry. After quenching with H₂O₂ and blocking with serum, primary antibodies against CD31, HIF-1 α , Runx2 and hypoxia marker were added to the sections. Antibody labeling was visualized by appropriate biotin-conjugated secondary antibodies followed by immunoperoxidase detection with the Vectastain ABC kit (Vector Laboratories, Linaris, Germany) and diaminobenzidine (DAB) substrate (Vector Laboratories). Counterstaining was performed with hematoxylin.

Statistical analysis - ANOVA tests were performed to assess the significance of differences among the experimental groups. The level of significance was set at $p < 0.01$ or $p < 0.05$. The results are represented as the mean \pm

the standard deviation (SD).

RESULTS

Runx2 enhances the stability of HIF-1 α protein under normoxic conditions - VEGF is primarily regulated by HIF-1 in response to hypoxia. Hypertrophic chondrocytes in growth plates express VEGF even where no evidence of hypoxia is detectable via immunohistochemistry with a hypoxic probe (4). VEGF mRNA is expressed by a Runx2 transcription factor-independent mechanism by HIF-1 α under normoxic conditions (30). Furthermore, HIF-1 α is stabilized and activated under both hypoxic and normoxic conditions (34). Thus, we hypothesized that Runx2 expressed in hypertrophic chondrocytes plays a role in the hypoxia-independent increase in HIF-1 α , and we investigated whether Runx2 regulates the expression and function of HIF-1 α in hypertrophic chondrocytes.

Initially, we prepared Runx2-overexpressing chondrocytes via stable transfection with a full-length Runx2 plasmid in ATDC5 murine chondrocytes. Interestingly, when overexpressing Runx2, ATDC5 cells experiencing normal oxygen levels displayed enhanced HIF-1 α stability relative to control cells (Fig. 1A). We next introduced the *RUNX2* gene into normoxic HEK293 cells and measured the expression of the HIF-1 α protein. The expression of HIF-1 α was increased by the overexpression of Runx2 under normoxic conditions (Fig. 1B, second lane), but to a lesser extent than in untransfected cells under hypoxic conditions (Fig. 1B, third lane). To determine whether Runx2 increased HIF-1 α expression at the transcriptional level, we analyzed HIF-1 α mRNA expression. Runx2 overexpression did not alter the expression of HIF-1 α mRNA, indicating that Runx2 did not increase HIF-1 α expression at the transcriptional level (Fig. 1B). To determine the level of HIF-1 α in response to Runx2 overexpression, we next measured HIF-1 α at 12 to 60 h after Runx2 transfection. HIF-1 α levels paralleled the Runx2 levels under normoxic conditions at the indicated times (Fig. 1C). Increasing levels of Runx2 significantly increased HIF-1 α protein levels

(Fig. 1D). These results suggest that Runx2 regulates the stability of HIF-1 α at the protein rather than the mRNA level.

To determine whether new protein synthesis is necessary for the regulation of HIF-1 α stability, we treated cells with cyclohexamide (CHX), a blocker of *de novo* protein synthesis. As shown in Fig. 1E, the HIF-1 α protein level was increased in the presence of Runx2 even under CHX treatment. This suggests that new protein synthesis was not responsible for Runx2-induced stabilization of HIF-1 α . From these results, we can infer that Runx2 enhances HIF-1 α stability at the post-translational level without new protein synthesis.

Runx2 enhances the nuclear translocation of HIF-1 α - For transactivation of HIF-1 α , HIF-1 α must translocate into the nucleus. Therefore, we analyzed whether Runx2 influenced the subcellular localization of HIF-1 α using an immunofluorescence assay. Using a GFP-fused HIF-1 α plasmid (pEGFP-HIF-1 α), nuclear accumulation of HIF-1 α was observed in the presence of Runx2 (Fig. 2A). HIF-1 α was barely detectable in the cytosol in the absence of desferrioxamine (DFX), a hypoxia-mimetic agent, whereas it accumulated only in the nucleus in the presence of DFX (Fig. 2A). Similarly, the level of HIF-1 α was both enhanced and redistributed into the nucleus when Runx2 was overexpressed. Cells showing higher expression of Runx2 (arrow) demonstrated stronger HIF-1 α nuclear translocation than cells expressing little (arrowheads) or no Runx2 (dashed arrows) (Fig. 2A, bottom images). The nuclear localization of Runx2 and HIF-1 α was further confirmed in the cytoplasmic and nuclear fractions by western blot analysis, as shown in Fig. 2B. The relative expression of nuclear HIF-1 α in control and Runx2-transfected cells is also shown in Fig. 2B, with higher expression levels detected in the Runx2-transfected cells. These results demonstrate that Runx2 increases the translocation of HIF-1 α into the nucleus and further suggest that Runx2 and HIF-1 α may interact there.

Runx2 interacts with HIF-1 α in vivo - Next, we

examined whether HIF-1 α and Runx2 physically associate with each other, which would facilitate the cross-talk between these two proteins. The interaction between HIF-1 α and Runx2 was determined after immunoprecipitating Runx2-overexpressing ATDC5 cells with a HIF-1 α antibody and subjecting the cell lysate to western blot analysis with Runx2 antibody (Fig. 3A). The interaction was also evaluated after transfection of the 3Myc-Runx2 expression plasmid into HEK293 cells (Fig. 3B). When cell extracts were immunoprecipitated with an anti-HIF-1 α antibody, Runx2 was successfully co-immunoprecipitated in the Runx2-overexpressing cells. Conversely, HIF-1 α was co-immunoprecipitated when Runx2-transfected cells were immunoprecipitated with an anti-Myc antibody (Fig. 3B). These results confirmed that HIF-1 α and Runx2 physically interact *in vivo*. To analyze the structural domain involved in this interaction, the cells were transfected with a GST-fused HIF-1 α deletion chimera plasmid. Immunoprecipitation experiments showed that Runx2 interacted with the ODDD and the full-length HIF-1 α protein, which is known to bind to ARNT or p300. However, Runx2 did not interact with the N-terminal activation domain (N-TAD)- or C-terminal activation domain (C-TAD)-containing HIF-1 α (Fig. 3C).

Runx2 competes with pVHL for binding to ODDD to block HIF-1 α degradation - The association of pVHL and HIF-1 α under normoxic conditions is triggered by the hydroxylation of prolines and the acetylation of lysine residues within the ODDD (34). When we transfected HEK293 cells with GST-fused HIF-1 α deletion chimeras and the pVHL full-length plasmid, the GST-HIF-1 α -ODDD (402 to 603 aa) was strongly bound to pVHL in a manner similar to full-length HIF-1 α ; in contrast, other segments showed no binding to pVHL (data not shown). Because Runx2 and pVHL interacted with the same domain (ODDD) of HIF-1 α , we investigated competitive binding to HIF-1 α of Runx2 vs. pVHL. GST-HIF-1 α -ODDD (402-603 aa) bound to pVHL, whereas the overexpression of Runx2 decreased pVHL binding to the ODDD (Fig. 4A). Conversely, the addition of the pVHL

expression plasmid decreased Runx2 binding to GST-ODDD-HIF-1 α in a dose-dependent manner (Fig. 4B). These data indicate that Runx2 and pVHL compete for binding to residues 402-603 of ODDD-HIF-1 α , which encompass the ODDD. To examine the regulatory role of Runx2 in its interaction with HIF-1 α -pVHL, we performed an *in vitro* binding assay. Runx2 interacted with HIF-1 α (Fig. 4C, second lane) and thereby inhibited the HIF-1 α -pVHL complex formation (Fig. 4C, last lane). This result indicates that Runx2 competes with pVHL for HIF-1 α binding.

Next, we attempted to determine whether Runx2 regulates the interaction of HIF-1 α with pVHL. As shown in Fig. 4D, when cells were treated with the proteasome inhibitor MG132, binding between HIF-1 α and pVHL was strongly detected, but it was largely diminished in the presence of either Runx2 or hypoxia. However, Runx2 inhibited the interaction between HIF-1 α and pVHL in the presence of MG132, suggesting that Runx2 suppresses the recruitment of pVHL to the HIF-1 α protein.

To further examine whether Runx2 induces HIF-1 α expression through the inhibition of proteasomal degradation, HEK293 cells were transfected with a Runx2 expression plasmid in either the presence or absence of MG132. After whole-cell extracts were immunoprecipitated with an anti-HIF-1 α antibody, ubiquitinated HIF-1 α was detected with an anti-ubiquitin antibody. As expected, the overexpression of Runx2, as well as hypoxia, dramatically suppressed HIF-1 α ubiquitination compared with ubiquitination in MG132-treated control cells (Fig. 4E). Collectively, these results demonstrate that Runx2 promotes HIF-1 α accumulation by inhibiting the interaction of pVHL and ODDD-HIF-1 α , suppressing HIF-1 α ubiquitination and degradation.

Runx2 regulates HIF-1 α independently from PHD - The result that pVHL binding to HIF-1 α was diminished by Runx2 prompted us to investigate whether Runx2 decreases the prolyl hydroxylation and lysine acetylation of ODDD-HIF-1 α . An examination of PHD1, 2, 3, and ARD1 mRNA levels in Runx2 overexpressing cells revealed that no substantial change in

mRNA expression was observed for any of these transcripts relative to control cells (Fig. 5A). Furthermore, the expression of hydroxylated HIF-1 α was not altered by Runx2 overexpression (Fig. 5B). These results suggest that Runx2 regulates HIF-1 α expression in a manner that is independent of hydroxylation by PHDs.

Runx2 potentiates the transcriptional activity of HIF-1 and angiogenesis - To confirm the role of the cross-talk between Runx2 and HIF-1 α , we measured the transcriptional activity of HIF-1 α by using a hypoxia response element (HRE)-luciferase reporter construct under the control of the VEGF or erythropoietin (EPO) promoter. Cotransfection of a VEGF-luciferase (luc) or an EPO-luc reporter gene with the Runx2 expression plasmid in HEK293 cells led to a 1.8- to 2.2-fold increase in reporter activity relative to those observed under hypoxic conditions (Fig. 6A). Expression of Glut-1, enolase, aldolase C and VEGF mRNA and secreted VEGF protein were significantly increased by Runx2 overexpression in a manner comparable to the increases induced by hypoxia (Fig. 6B and C). These results indicate that Runx2 enhances the transcriptional activity of HIF-1, even in the absence of hypoxic stress.

Based on the results that Runx2 stabilizes HIF-1 α and increases its transactivation, we investigated whether Runx2 showed angiogenic activities by performing *in vitro* angiogenesis assays using CM derived from Runx2-overexpressing cells (CM-Runx2). CM-Runx2 markedly increased the proliferation (Fig. 6D) and migration (Fig. 6E) of HUVECs relative to control CM. Furthermore, the CM from mock-transfected cells cultured under hypoxic conditions and CM-Runx2 both enhanced the formation of complex, elongated networks of HUVECs (Fig. 6F). When a VEGF-neutralizing antibody was added to the CM-Runx2, tube-like structures became disrupted and incomplete in a manner reminiscent of the normoxic control (Fig. 6F). These results support the idea that Runx2 is a potent inducer of angiogenesis, which acts through HIF-1 α -dependent transactivation of VEGF, even under normoxic conditions.

HIF-1 α is expressed in hypertrophic

chondrocytes, whereas Runx2 is expressed in the murine fetal growth plate - To investigate whether HIF-1 α is expressed where Runx2 is expressed in the growth plate, tibia long bone of wild-type, Runx2-heterozygote and Runx2-knockout mice (E15.5) were sectioned and processed for immunohistochemical detection of Runx2 and HIF-1 α . A marker of hypoxia, pimonidazole, was injected intravenously into the mice 3 h before sacrifice and was subsequently detected in the growth plate with a hypoxic probe (4). Runx2 was detected in E15.5 mice embryos in hypertrophic chondrocytes, whereas HIF-1 α was expressed in wild-type mice (Fig. 7B). However, in Runx2^{-/-} mice, expression of HIF-1 α was absent, corroborating the results that Runx2 stabilized HIF-1 α . Interestingly, hypoxic regions were not found in the hypertrophic chondrocytes but were present in proliferating chondrocytes (Supplementary Fig. S1). This indicates that HIF-1 α expression is independent of hypoxia. This result strongly supports our initial hypothesis and subsequent finding that, in endochondral ossification, HIF-1 α is both activated and stabilized by the key osteogenic transcription factor Runx2.

DISCUSSION

Here, we show that Runx2 stabilizes HIF-1 α through direct binding to the ODDD of HIF-1 α , thereby competitively blocking its interaction with pVHL. The stabilization of HIF-1 α by Runx2 in hypertrophic chondrocytes stimulates transcription of VEGF, followed by the invasion of blood vessels and maturation of bone formation. In endochondral bone formation, chondrocyte hypertrophy is essential for apoptosis and for the invasion of blood vessels, osteoclasts and other mesenchymal cells that are required for longitudinal bone growth (13). Invasion of blood vessels into cartilage is related to the expression of VEGF, the most potent angiogenic factor that is regulated by HIFs in embryonic development and angiogenic diseases (30).

In fact, it has been reported that Runx2 upregulates *VEGF* gene expression by binding to the *VEGF* promoter region (30). As a

transcription factor, Runx2 can increase *VEGF* gene expression at the transcriptional level. From our results, Runx2 stabilizes HIF-1 α and then increases the transcription of *VEGF* through HIF-1 α activation. Therefore, Runx2 has a dual mechanism to directly increase VEGF as a transcription factor and to indirectly upregulate VEGF via the stabilization of HIF-1 α . This dual function of Runx2 to increase VEGF might finely regulate and tune the vascular invasion spatio-temporally in developing hypertrophic chondrocytes, in HIF-1 α -dependent as well as HIF-1 α -independent ways.

Hypoxia is a strong stimulus, but not the only stimulus, that induces the *VEGF* gene as well as HIF-1 α . It is well established that HIF-1 can also be activated by conditions other than hypoxia. The regulatory subunit of HIF-1, HIF-1 α , is continuously degraded under normoxic conditions. In contrast, reduced prolyl hydroxylase activity under hypoxic conditions stabilizes HIF-1 α by reducing its ubiquitin/proteasome-dependent degradation (18). However, several growth factors, hormones and cytokines have been shown to upregulate HIF-1 α protein levels in normoxia through mechanisms that generally differ from those operating at low oxygen concentrations (35). We showed here that an important role for Runx2 is as an additional inducer of HIF-1 α activity during endochondral bone formation. In general, these stimuli would act by increasing transcription of the gene that encodes HIF-1 α and/or translation of its mRNA without affecting protein stability, and could therefore cooperate with hypoxia to induce HIF-1 α accumulation in an additive manner. However, our data indicate no additive effect on HIF-1 α accumulation or activity when HEK293 cells were transfected with Runx2 under hypoxic conditions (data not shown). Our findings suggest that Runx2 does not affect HIF-1 α production, as opposed to other non-hypoxic stimuli. Instead, it appears that Runx2 shares mechanistic similarities with hypoxia, involving increased protein stability, to induce HIF-1 α accumulation.

Runx2 is a master regulator of endochondral bone formation through hypertrophic

chondrocyte differentiation. Mice missing Runx2 have no osteoblasts and demonstrate abnormal chondrocyte maturation because of the absent expression of osteopontin and matrix metalloproteinase 13, which are normally expressed in late hypertrophic chondrocytes (36). The deficiency of Runx2 might lead to the failure of chondrocyte maturation because the stabilization of HIF-1 α and the downstream VEGF expression necessary to recruit blood vessels into the hypertrophic chondrocyte would not occur. The incomplete formation of blood vessels cannot provide a functional link with mesenchymal cells in bone formation. The inhibition of HIF-1 α function impairs osteoblast proliferation, while osteoblasts continue to differentiate normally. On the other hand, osteoblasts lacking Runx2 proliferate normally, while their differentiation is impaired. More precise investigations regarding the collaboration between Runx2 and HIF-1 α in context-dependent and spatio-temporal manners should be further determined in endochondral bone development. So far, we suggest that Runx2 regulates bone maturation factors as well as HIF-1 α in the chondrocyte for the proper development of endochondral bone formation.

In Runx family, it has been reported that RUNX1 and Runx2 physically interact with HIF-1 α and regulate the transcription function of HIF-1 α (37, 38). Dual inhibition of Runx2 and HIF-1 α synergistically aggravate bone formation (39). We showed here that Runx2 has a function to stabilize the HIF-1 α protein by blocking pVHL binding to HIF-1 α . Runx2 also activates its transcription function to increase VEGF in developing mouse hypertrophic chondrocytes, including under normoxic conditions. It has also been reported that RUNX3 suppresses VEGF expression (40), but Runx2 induces VEGF expression (30). Therefore, Runx family proteins regulate angiogenesis differently, in that RUNX1 and RUNX3 inhibit angiogenesis, while Runx2 stimulates angiogenesis. It is interesting that the hypothetical functions of RUNX1 and RUNX3 are as tumor suppressors, and that Runx2 functions as an oncogenic protein (41). Therefore, in the regulation of angiogenic molecules, such as VEGF or HIF-1 α , only Runx2

among the Runx family members has a “positive” function. It is therefore consistent that Runx2 is overexpressed in tumors, such as chondrosarcoma (41).

In developing murine long bone growth plates, proliferating chondrocytes express HIF-1 α and hypoxia markers (4). However, HIF-1 α is also expressed in hypertrophic chondrocytes in non-hypoxic regions, where Runx2 is coexpressed in wild-type and Runx2 $^{+/-}$ mice. Moreover, Runx2 $^{-/-}$ mice displayed no expression of hypoxic markers or Runx2 in hypertrophic chondrocytes, although HIF-1 α was expressed in the proliferating zone (Fig. 7, Fig. S1). These findings provide convincing evidence that HIF-1 α is a downstream target of Runx2 in bone development in normoxic regions. CD31-positive endothelial cells were found in hypertrophic chondrocytes, implying active invasion of blood vessels into hypertrophic zones in wild-type and Runx2 $^{+/-}$ mice. However, no blood vessel invasion into extended hypertrophic zones was observed in Runx2 $^{-/-}$ mice, indicating that an absence of Runx2 suppressed angiogenesis by rendering HIF-1 α unstable and reducing the expression of VEGF. In the development of osteoarthritis, hypoxia increases HIF-2 α , which contributes to stem cell-derived chondrogenesis (42). Therefore, the induction of HIF- α by hypoxia or other regulators may be cell- or context-specific.

Collectively, the results of this study lead us to propose that Runx2 directly binds to and stabilizes the HIF-1 α protein by reducing the interaction between HIF-1 α and pVHL, leading to the induction and maintenance of microvessels during endochondral bone formation. In conclusion, we suggest a novel mechanism whereby HIF-1 α is regulated by the Runx2 transcription factor during endochondral bone formation. Runx2 might therefore be a suitable target for therapies that seek to suppress angiogenesis in various bone disorders and solid tumors.

Acknowledgments

We thank Dr. Suk-Chul Bae (Chungbuk National University, Korea) for generating the HA- and Myc-tagged Runx2 plasmids in the pCS4 vector (pCS4-3HA-Runx2, pCS4-3Myc-Runx2).

REFERENCES

1. Carmeliet, P., and Jain, R.K. (2000) *Nature* **407**, 249-257
2. Brahimi-Horn, C., Berra, E., and Pouyssegur, J. (2001) *Trends Cell Biol.* **11**, S32-S36
3. Erlebacher, A., Filvaroff, E. H., Gitelman, S. E., and Derynck, R. (1995) *Cell* **80**, 371-378
4. Schipani, E. (2005) *Semin. Cell Dev. Biol.* **16**, 539-546
5. Iyama, K., Ninomiya, Y., Olsen, B. R., Linsenmayer, T. F., Trelstad, R. L., and Hayashi, M. (1991) *Anat. Rec.* **229**, 462-472
6. Ninomiya, Y., Gordon, M., van der Rest, M., Schmid, T., Linsenmayer, T., and Olsen, B. R. (1986) *J. Biol. Chem.* **261**, 5041-5050
7. Vortkamp, A., Lee, K., Lanske, B., Segre, G. V., Kronenberg, H. M., and Tabin, C. J. (1996) *Science* **273**, 613-622
8. Trueta, J., and Buhr, A. J. (1963) *J. Bone Joint Surg. Br.* **45**, 572-581
9. Trueta, J., and Amato, V. P. (1960) *J. Bone Joint Surg. Br.* **42-B**, 571-587
10. St-Jacques, B., Hammerschmidt, M., and McMahon, A. P. (1999) *Genes Dev.* **13**, 2072-2086
11. Zelzer, E., Mamluk, R., Ferrara, N., Johnson, R. S., Schipani, E., and Olsen, B. R. (2004) *Development* **131**, 2161-2171
12. Gerber, H. P., Vu, T. H., Ryan, A. M., Kowalski, J., Werb, Z., and Ferrara, N. (1999) *Nat. Med.* **5**, 623-628
13. Kuettner, K. E., and Pauli, B. U. (1983) *Ciba. Found Symp.* **100**, 163-173
14. Descalzi, Cancedda, F., Melchiorri, A., Benelli, R., Gentili, C., Masiello, L., Campanile, G., Cancedda, R., and Albin, A. (1995) *Eur. J. Cell Biol.* **66**, 60-68
15. Iyer, N. V., Kotch, L. E., Agani, F., Leung, S. W., Laughner, E., Wenger, R. H., Gassmann, M., Gearhart, J. D., Lawler, A. M., Yu, A. Y., and Semenza, G. L. (1998) *Genes Dev.* **12**, 149-162
16. Semenza, G. L. (2001) *Cell* **107**, 1-3
17. Jiang, B. H., Rue, E., Wang, G. L., Roe, R., and Semenza, G. L. (1996) *J. Biol. Chem.* **271**, 17771-17778
18. Salceda, S., and Caro, J. (1997) *J. Biol. Chem.* **272**, 22642-22647
19. Ohh, M., Park, C. W., Ivan, M., Hoffman, M. A., Kim, T. Y., Huang, L. E., Pavletich, N., Chau, V., and Kaelin, W. G. (2000) *Nat. Cell Biol.* **2**, 423-427
20. Masson, N., Willam, C., Maxwell, P. H., Pugh, C. W., and Ratcliffe, P. J. (2001) *EMBO J.* **20**, 5197-5206
21. Ivan, M., Kondo, K., Yang, H., Kim, W., Valiando, J., Ohh, M., Salic, A., Asara, J. M., Lane, W. S., and Kaelin, W. G. (2001) *Science* **292**, 464-468
22. Schipani, E., Ryan, H. E., Didrickson, S., Kobayashi, T., Knight, M., and Johnson, R. S. (2001) *Genes Dev.* **15**, 2865-2876
23. Provot, S., and Schipani, E. (2007) *Ann. N. Y. Acad. Sci.* **1117**, 26-39
24. Provot, S., Zinyk, D., Gunes, Y., Kathri, R., Le, Q., Kronenberg, H. M., Johnson, R. S., Longaker, M. T., Giaccia, A. J., and Schipani, E. (2007) *J. Cell Biol.* **177**, 451-464
25. Riddle, R. C., Khatri, R., Schipani, E., and Clemens, T. L. (2009) *J. Mol. Med.* **87**, 583-590
26. Karsenty, G. (1999) *Genes Dev.* **13**, 3037-3051
27. Nakashima, K., Zhou, X., Kunkel, G., Zhang, Z., Deng, J. M., Behringer, R. R., and de Crombrughe, B. (2002) *Cell* **108**, 17-29
28. Mundlos, S., Otto, F., Mundlos, C., Mulliken, J. B., Aylsworth, A. S., Albright, S., Lindhout, D., Cole, W. G., Henn, W., Knoll, J. H., Owen, M. J., Mertelsmann, R., Zabel, B. U., and Olsen, B. R. (1997) *Cell* **89**, 773-779

29. Yoshida, C. A., Yamamoto, H., Fujita, T., Furuichi, T., Ito, K., Inoue, K., Yamana, K., Zanma, A., Takada, K., Ito, Y., and Komori, T. (2004) *Genes Dev.* **18**, 952-963
30. Zelzer, E., Glotzer, D. J., Hartmann, C., Thomas, D., Fukai, N., Soker, S., and Olsen, B. R. (2001) *Mech. Dev.* **106**, 97-106
31. Jeong, J. H., Jin, J. S., Kim, H. N., Kang, S. M., Liu, J. C., Lengner, C. J., Otto, F., Mundlos, S., Stein, J. L., van Wijnen, A. J., Lian, J. B., Stein, G. S., and Choi, J. Y. (2008) *J. Cell Physiol.* **217**, 511-517
32. Jang, G. H., Park, I. S., Yang, J. H., Bischoff, J., and Lee, Y. M. (2010) *FEBS Lett.* **584**, 141-146
33. Jung, M. H., Lee, S. H., Ahn, E. M., and Lee, Y. M. (2009) *Carcinogenesis* **30**, 655-661
34. Lee, J. W., Bae, S. H., Jeong, J. W., Kim, S. H., and Kim, K. W. (2004) *Exp. Mol. Med.* **36**, 1-12
35. Fukuda, R., Hirota, K., Fan, F., Jung, Y. D., Ellis, L. M., and Semenza, G. L. (2002) *J. Biol. Chem.* **277**, 38205-38211
36. Kronenberg, H. M. (2003) *Nature.* **423**, 332-336
37. Peng, Z. G., Zhou, M. Y., Huang, Y., Qiu, J. H., Wang, L. S., Liao, S. H., Dong, S., and Chen, G. Q. (2008) *Oncogene* **27**, 839-847
38. Kwon TG, Zhao X, Yang Q, Li Y, Ge C, Zhao G, Franceschi RT. (2011) *J. Cell Biochem.* **112**, 3582-93.
39. Lin, L., Shen, Q., Leng, H., Duan, X., Fu, X., Yu, C. (2011) *Mol Ther.* **19**, 1426-32
40. Peng, Z., Wei, D., Wang, L., Tang, H., Zhang, J., Le, X., Jia, Z., Li, Q., and Xie, K. (2006) *Clin. Cancer Res.* **12**, 6386-6394
41. Anglin, I., and Passaniti, A. (2004) *Cancer Treat. Res.* **119**, 189-215
42. Khan, W.S., Adesida, A.B., Hardingham, T.E. (2007) *Arthritis Res Ther* **9**, R55.

FOOTNOTES

*This work was supported by a Korea Science and Engineering Foundation (KOSEF) grant funded by the Korean government (Ministry of Science and Technology (MOST); No. R01-2006-000-11046-0) and by the Mid-career Researcher Program through the National Research Foundation of Korea (NRF) grants funded by the Ministry of Education, Science and Technology (MEST; No. 2010-0026741 and 2009-0084887).

^{1,2}To whom correspondence may be addressed: You Mie Lee, Ph.D., College of Pharmacy, Kyungpook National University, #80 Daehak-ro, Buk-gu, Daegu, 702-701, Republic of Korea. Tel: +82-53-950-8566, Fax: +82-53-950-8557, E-mail: lym@knu.ac.kr.

FIGURE LEGENDS

FIGURE 1. Runx2 increases HIF-1 α stability. A, ATDC5 cells were transfected with Runx2 full-length expression or mock plasmids and selectively cultured in G418-containing medium for 2 weeks. HIF-1 α protein levels were examined by western blot analysis. B, HEK293 cells were transfected with the 3Myc-Runx2 expression plasmid or exposed to hypoxia (1% O₂). The resulting changes in HIF-1 α and Runx2 protein levels were examined by western blot analysis with mouse anti-human HIF-1 α and mouse anti-Myc antibodies. Semi-quantitative RT-PCR analysis was carried out with specific primers for HIF-1 α and β -actin. α -tubulin and β -actin were used as the internal controls. C, HEK293 cells were transfected with the 3Myc-Runx2 plasmid for the indicated times. HIF-1 α and Runx2 protein levels were examined by western blotting with the same antibodies used in B. α -tubulin was used as the internal control. D, HEK293 cells were transfected with various doses of the 3Myc-Runx2 expression plasmid. HIF-1 α and Runx2 protein levels were examined by western blot analysis with the same antibodies used in B. α -tubulin was used as the internal control. E, HEK293 cells were transfected with the 3Myc-Runx2 expression plasmid or mock plasmid. Twenty-four hours after transfection, 60 μ g/ml CHX was added into the media for 10 and 60 min. HIF-1 α and Runx2

protein levels were examined by western blot analysis. β -actin was used as the internal control. Levels of HIF-1 α and Runx2 were quantified using the ImageJ program (NIH, Bethesda, MO) after being normalized to those of β -actin or α -tubulin; the results were plotted. * $p < 0.01$ vs. control or indicated group.

FIGURE 2. Runx2 increases the protein level and translocation of HIF-1 α into the nucleus. A, HEK293 cells were transfected with GFP-HIF-1 α and/or 3Myc-Runx2-full-length plasmids. Transfected cells were treated with or without desferrioxamine (100 μ M) for 24 h. Runx2 expression was visualized with anti-Myc primary and Texas Red-conjugated secondary antibodies. DAPI was used for staining the nuclei. A, The white arrow shows cells with high expression of Runx2; arrowheads denote cells with intermediate expression of Runx2; and dashed arrows indicate cells with little or no expression of Runx2. B, HEK293 cells were transfected with mock or 3Myc-Runx2 plasmids. Cytoplasmic and nuclear fractions were extracted, and the expression levels of HIF-1 α and Runx2 were analyzed by western blot analysis. * $p < 0.01$ vs. control.

FIGURE 3. Physical interaction between Runx2 and the ODDD of HIF-1 α *in vivo*. A, ATDC5 cells that stably overexpressed Runx2 were immunoprecipitated (IP) with anti-HIF-1 α antibody and immunoblotted (IB) with anti-Runx2 antibody. B, HEK293 cells were transfected with the 3Myc-Runx2 expression plasmid. After the HIF-1 α and 3Myc-Runx2 proteins were immunoprecipitated from transfected cell extracts using anti-HIF-1 α or anti-Myc antibodies, Runx2 and HIF-1 α protein contents were analyzed by western blot analysis. C, Structures of the HIF-1 α protein and its deletion derivatives are schematically shown in the upper panel. Lower panel: HEK293 cells were transfected with each GST-HIF-1 α deletion construct and 3Myc-Runx2. Whole-cell lysates were immunoprecipitated with an anti-GST antibody and probed with an anti-Myc antibody. The expression of GST-HIF-1 α deletions and 3Myc-Runx2 was analyzed by western blot analysis. Cells were transfected with identical amounts of Runx2, and the expression levels were subsequently confirmed.

FIGURE 4. Runx2 competes with pVHL for binding to HIF-1 α and blocks the ubiquitination of HIF-1 α . A, HEK293 cells were transfected with GST-HIF-1 α -ODDD and HA-pVHL. Cells were also transfected with 3Myc-Runx2 to compete with pVHL for binding to GST-HIF-1 α -ODDD. Whole cell lysates were immunoprecipitated with an anti-GST antibody, probed with an anti-Myc antibody, and subsequently analyzed by western blot analysis to detect bound Runx2. B, HEK293 cells were transfected with GST-HIF-1 α -ODDD and 3Myc-Runx2. The cells were cotransfected with pVHL at the indicated doses to compete with Runx2 for binding to GST-HIF-1 α -ODDD. Whole cell lysates were immunoprecipitated with an anti-GST antibody and probed with anti-HA or anti-GST antibodies. C, *In vitro* binding assay to detect the HIF-1 α and pVHL interaction. GFP-HIF-1 α was incubated with HA-Runx2 or HA-pVHL *in vitro*. HA-Runx2 and HA-pVHL were pulled-down with anti-GFP-conjugated magnetic beads and immunoblotted using an anti-HA antibody. D, HEK293 cells were cotransfected with 3Myc-Runx2 full-length and HA-pVHL plasmids. After transfection, the cells were treated with or without 10 μ M MG132 or subjected to hypoxia. Whole cell lysates were immunoprecipitated with an anti-HA antibody and then probed with an anti-HIF-1 α antibody. The pVHL levels were determined with an anti-HA antibody to ensure an equivalent amount of transfected plasmid. E, After HEK293 cells were transfected with mock or Runx2 full-length plasmids, the cells were treated with or without 10 μ M MG132 or subjected to hypoxia. After immunoprecipitation of HIF-1 α from whole cell extracts, ubiquitinated forms of HIF-1 α were detected using an anti-ubiquitin antibody. The HIF-1 α level was determined with an anti-HIF-1 α antibody. * $p < 0.01$ vs. control.

FIGURE 5. Runx2 does not alter the hydroxylation status of HIF-1 α . A, After transfection with the Runx2 full-length plasmid, PHD1-3 and ARD1 mRNA levels were determined by semi-quantitative RT-PCR. As an internal control, β -actin levels were also detected. B, HEK293 cells were

transfected with mock or Runx2 full-length plasmids and then treated with or without MG132 (10 μ M). Hydroxylated HIF-1 α was detected by immunoblotting. β -actin was used as an internal control.

FIGURE 6. The transcriptional and angiogenic activity of HIF-1 is enhanced by Runx2 through the induction of VEGF. A, HEK293 cells were cotransfected with the 3Myc-Runx2 expression plasmid and VEGF or an EPO promoter-driven reporter. After transfection, the cells were incubated at 21% O₂ or 1% O₂ for 24 h, and luciferase activity was determined. Relative luciferase activity was evaluated by normalization of β -galactosidase activity. * $p < 0.01$ vs. control. B, HEK293 cells were transfected with mock or 3Myc-Runx2 expression plasmids or exposed to hypoxia for 24 h. Semi-quantitative RT-PCR analysis was performed with specific primers for Glut-1, enolase, aldolase C, VEGF and β -actin. The band intensities were analyzed using ImageJ. The data are VEGF expression levels compared with each control after normalization to β -actin expression. * $p < 0.01$ vs. control. C, HEK293 cells were transfected with mock or Runx2 plasmids or subjected to hypoxic conditions. After 24 h of incubation, CM were collected and analyzed for the presence of VEGF by ELISA. * $p < 0.01$ vs. control. D, HEK293 cells transfected with mock or Runx2 plasmids were incubated with fresh M199 containing 10% FBS, and the resulting CM was collected at 24 h. HUVECs were treated with the CM from mock- or Runx2-transfected cells or hypoxia-treated cells, and then a [³H]-thymidine incorporation assay was performed. * $p < 0.01$ vs. control. E, HUVECs were treated with the CM from mock- (N.C.) or Runx2-transfected cells (N.Runx2), or the hypoxia control (H.C.). The cells were incubated in a transwell chamber previously coated with collagen IV and Matrigel for 16 h. The number of invaded cells was counted under a light microscope, and the mean values were plotted. * $p < 0.01$ vs. control. F, HUVECs were incubated for 24 h in the CM from Runx2-transfected cells (N.Runx2) with or without an antibody against VEGF (N.Runx2 + VEGF Ab). Alternatively, HUVECs were subjected to hypoxia (H.C.) in a 24-well culture plate previously coated with Matrigel. The cell morphology was observed for 24 h under the microscope and compared to the normal control (N.C.). Branching points were counted and plotted for quantification. * $p < 0.01$ vs. control. All experiments were performed in triplicate.

FIGURE 7. Expression of hypoxic markers, Runx2 and HIF-1 α , in hypertrophic chondrocytes in long bone growth plates among Runx2 wild-type, heterozygote and knockout mice at E15.5. A, A schematic diagram for developing growth plate cells in bone development. The boxed region corresponds to the immunohistochemistry result from murine bone from B and C. B, Immunohistochemical staining of Runx2 and HIF-1 α with optimal primary antibodies and FITC- or Texas Red-labeled secondary antibodies was performed in the wild-type fetal growth plate at E15.5 and observed under a fluorescent microscope. DAPI staining was then performed to visualize the nuclei. The arrow represents the same direction as in the schematic diagram. C, Expression of CD31 and HIF-1 α in the E15.5 wild-type (WT), Runx2 heterozygote (Runx2^{+/-}), and Runx2 knockout (Runx2^{-/-}) mice was detected by immunohistochemistry with optimal primary and secondary antibodies. The brown color was obtained by DAB staining. The white-lined inset corresponds to the red-boxed region enlarged by two-fold. Images were obtained using a magnification of 100X (scale bar: 100 μ m). D, The CD31-positive cells in the hypertrophic zone were counted and plotted. * $p < 0.01$.

Fig. 1

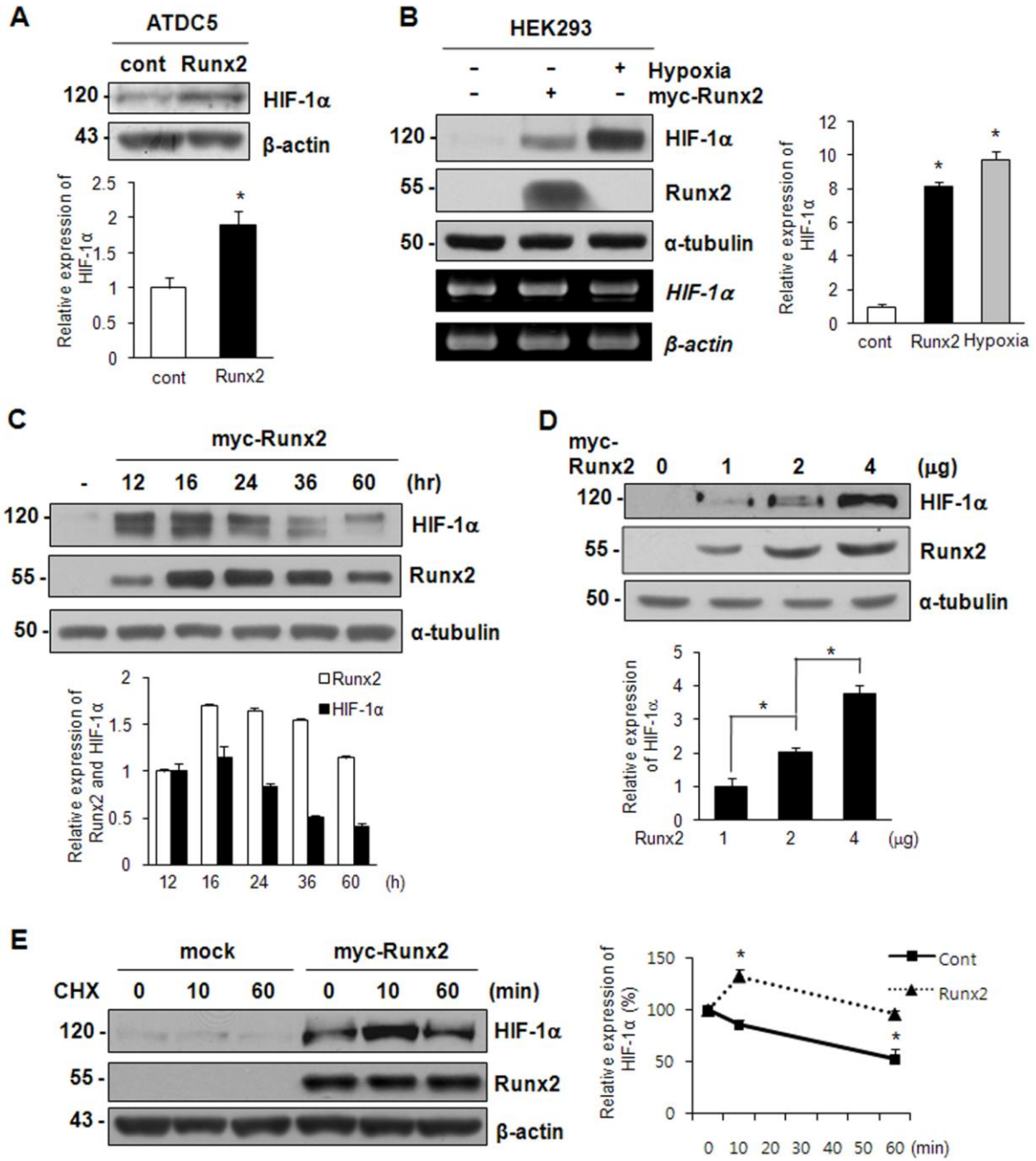


Fig.2

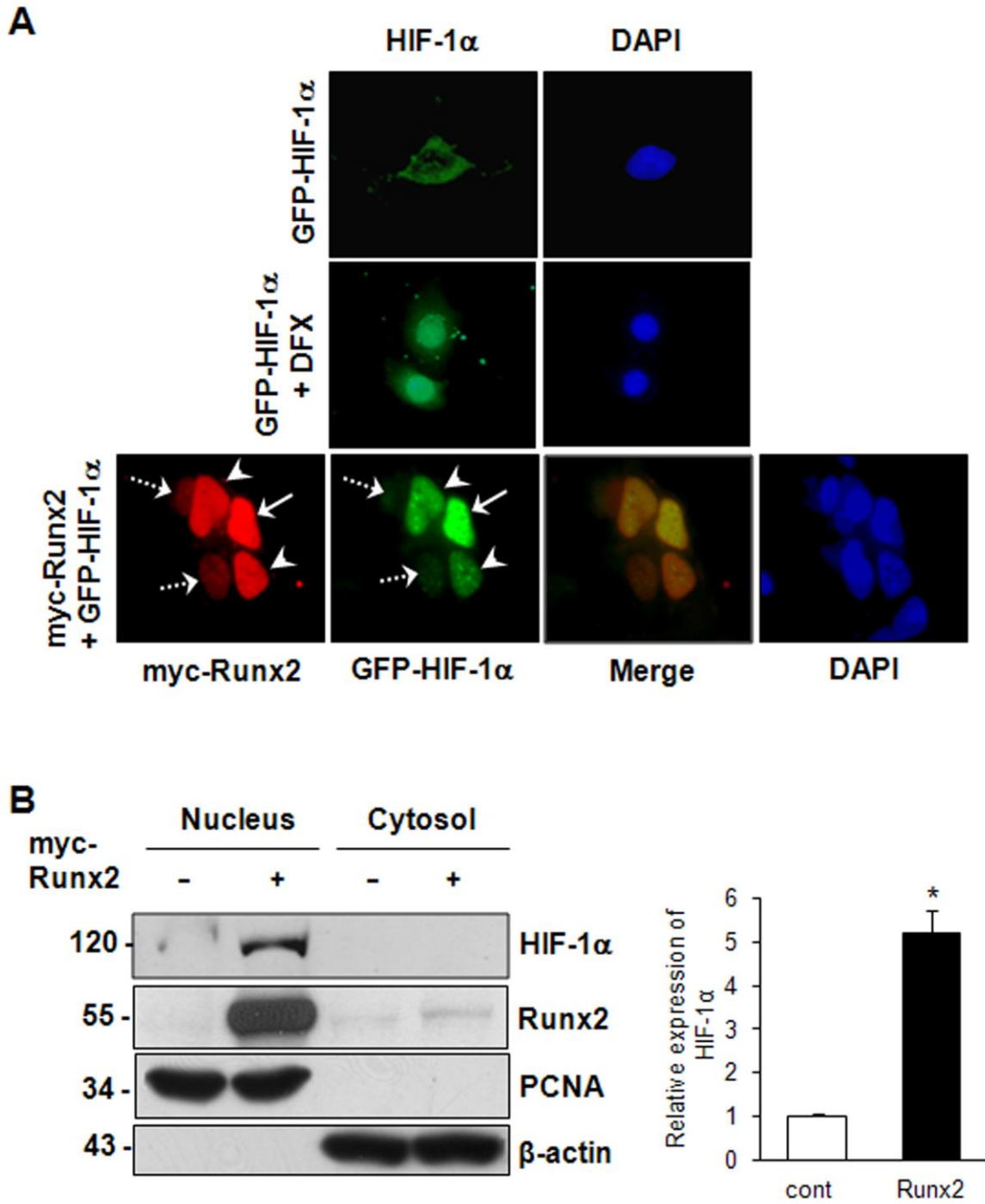


Fig. 3

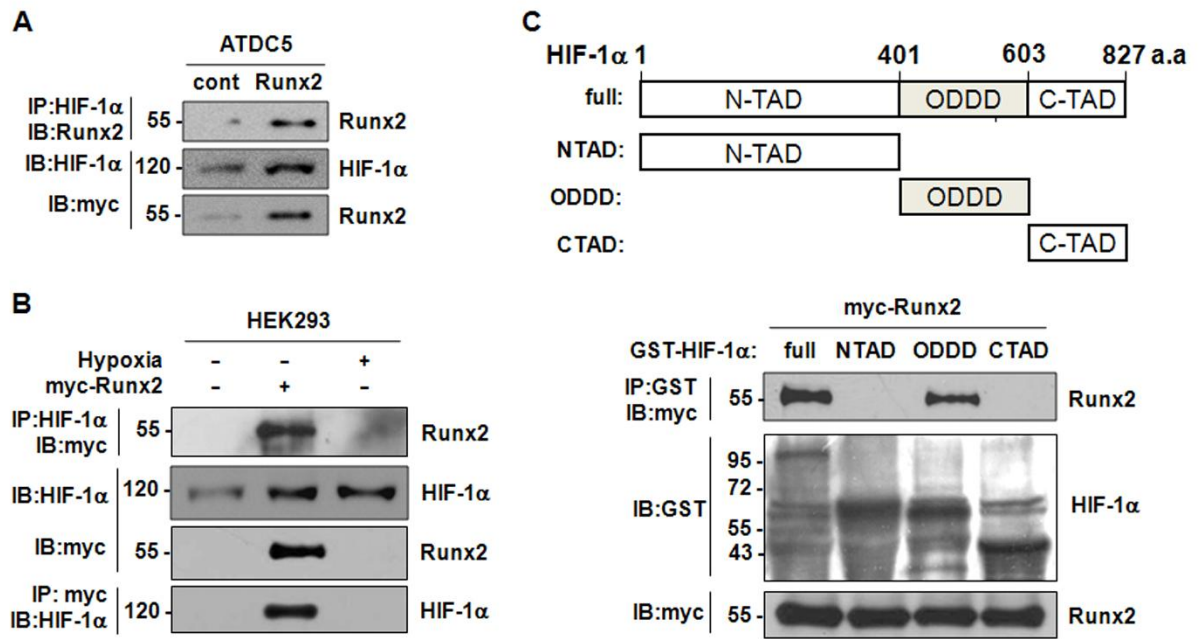


Fig.4

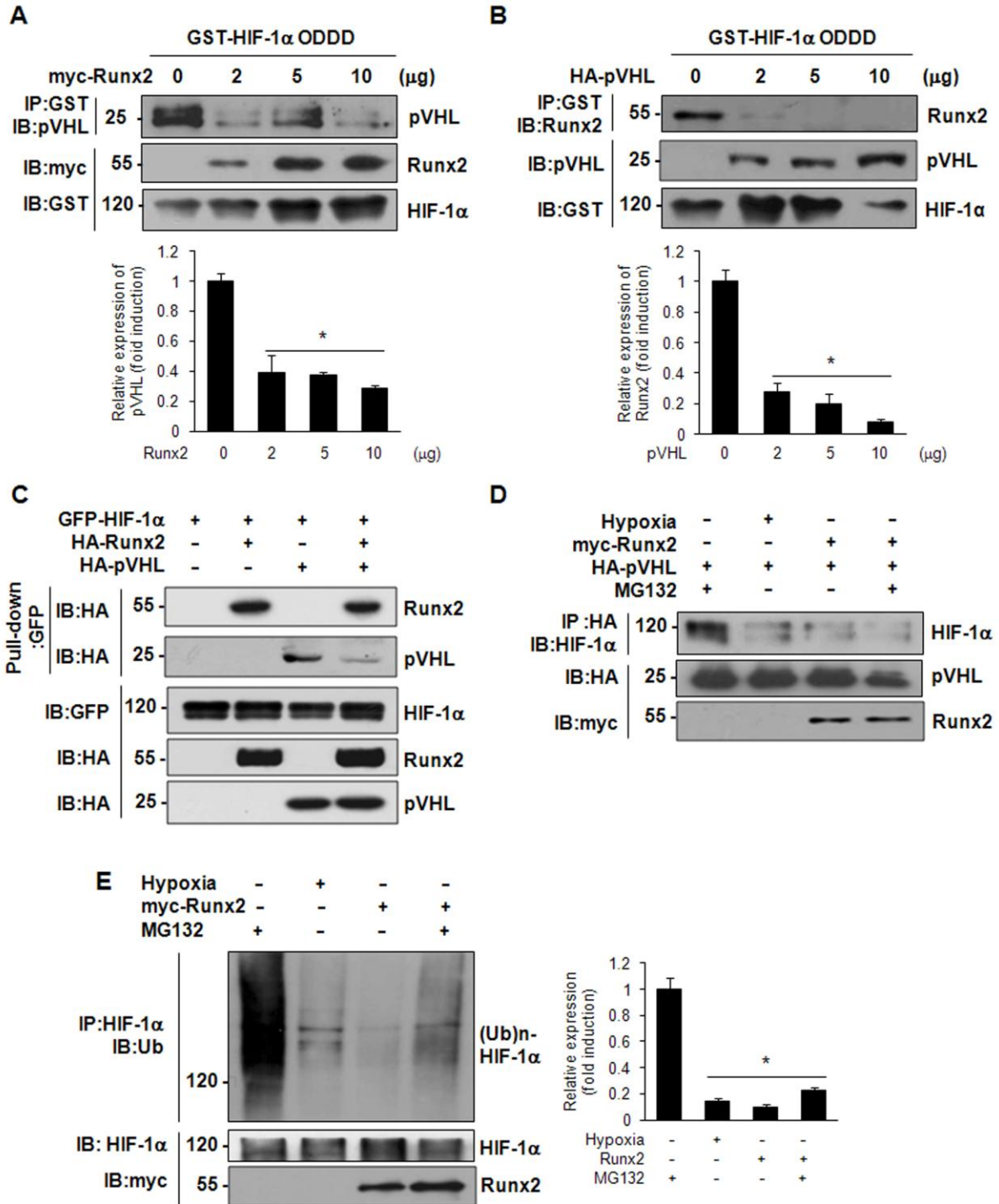


Fig. 5

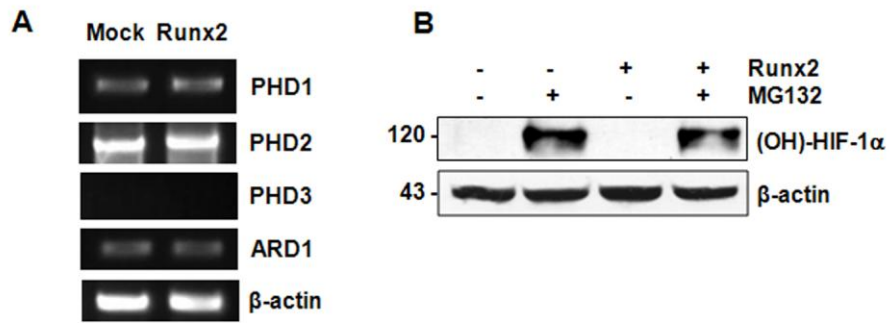


Fig. 6

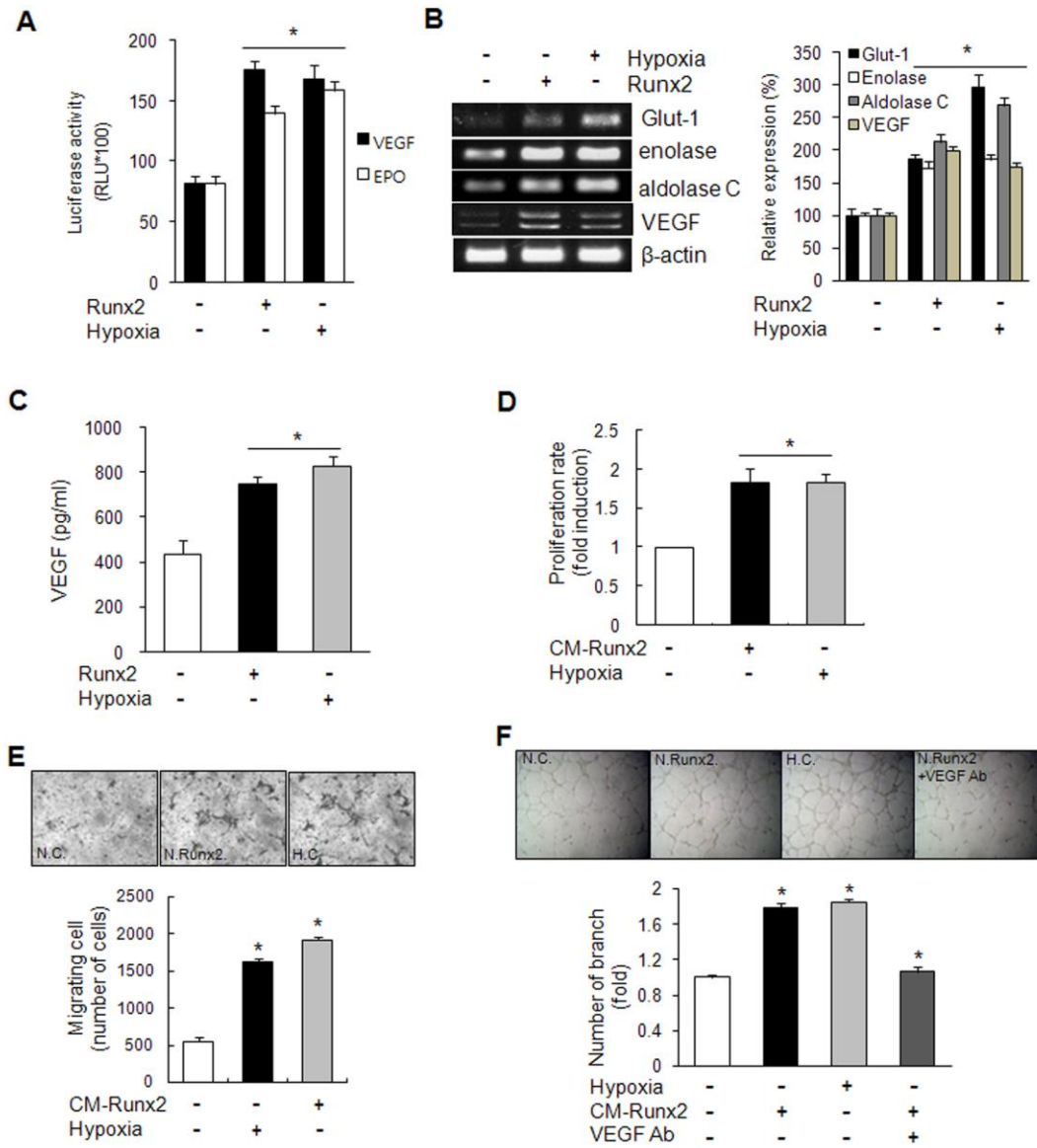


Fig. 7

